

**DEVELOPMENT OF NEAR-SEA-LEVEL
LANGLEY CALIBRATION ALGORITHM FOR
AEROSOL OPTICAL DEPTH MEASUREMENT**



JACKSON CHANG HIAN WUI

UMS
UNIVERSITI MALAYSIA SABAH

**SCHOOL OF SCIENCE AND TECHNOLOGY
UNIVERSITI MALAYSIA SABAH
2014**

**DEVELOPMENT OF NEAR-SEA-LEVEL
LANGLEY CALIBRATION ALGORITHM FOR
AEROSOL OPTICAL DEPTH MEASUREMENT**

JACKSON CHANG HIAN WUI



UMS
UNIVERSITI MALAYSIA SABAH

**THIS IS SUBMITTED IN FULFILLMENT FOR
THE DEGREE OF MASTER OF SCIENCE**

**SCHOOL OF SCIENCE AND TECHNOLOGY
UNIVERSITI MALAYSIA SABAH
2014**

DECLARATION

I hereby declare that the material in this thesis is my own except for quotations, excerpts, equations, summaries and references, which have been dully acknowledged.

26 February 2014

Jackson Chang HianWui
PS2011-8036



UMMS
UNIVERSITI MALAYSIA SABAH

CERTIFICATION

NAME : **JACKSON CHANG HIAN WUI**
MATRIC NO. : **PS2011-8036**
TITLE : **DEVELOPMENT OF NEAR-SEA-LEVEL LANGLEY
CALIBRATION ALGORITHM FOR AEROSOL OPTICAL
DEPTH MEASUREMENT**
DEGREE : **MASTER OF SCIENCE**
VIVA DATE : **18 FEBRUARY 2014**

DECLARED BY;

1. **SUPERVISOR**

Associate Professor Dr.Jedol Dayou

Signature



UMMS
UNIVERSITI MALAYSIA SABAH

2. **Co -SUPERVISOR**

Dr. Justin Sentian

ACKNOWLEDGEMENT

I wish to express my deepest gratitude and appreciation to my supervisors, Associate Professor Dr.Jedol Dayou and Dr. Justin Sentian of School of Science and Technology, Universiti Malaysia Sabah who had been patient enough to advise, guide and supervise me towards the completion of this thesis. Their continuous encouragement provided me the necessary impetus to complete the research and publish this thesis in some journals.

My special sense of gratitude is also expressed to my dearest family who had been supporting me throughout the past years particularly in moral and financial support. Finally, I wish to thank all my friends and e-VIBS lab members for their constructive ideas and encouragements throughout my master studies.

Jackson Chang Hian Wui
PS2011-8036



UMS
UNIVERSITI MALAYSIA SABAH

ABSTRACT

Aerosol optical depth (AOD) represents the total attenuation of solar terrestrial radiation caused by aerosol. In long-term monitoring networks, accurate measurement of AOD is difficult due to the lack of frequent calibration of the spectrometer. This is because conventional Langley calibration is usually performed at high mountains for clear and stable atmosphere and regular access to high altitudes is inefficient in terms of accessibility and economical prospects. Therefore, a near-sea-level Langley calibration algorithm is developed to allow frequent calibration feasible even at low altitude. It uses the combination of Perez-Du Mortier (PDM) model and statistical filter to constrain the Langley extrapolation to get closest possible extraterrestrial constant over a wide range of wavelengths. To further contain the wavelength-dependent error due to varying extraterrestrial constant, the Ratio Langley method is combined with the proposed algorithm to improve the prediction accuracy. In this way, more accurate AOD can be estimated by reanalysis of the calibrated volume spectrum using Beer-Lambert law. A total of 568 useful solar spectral data had been collected using ground-based spectrometer for the validation purposes. It is found that the AODs predicted by the proposed algorithm agree well to the reference values obtained from i-SMARTS model with high linearity and small error $<3\%$ for all wavelengths. The consistency of the proposed method is also validated with good result over two study areas ($n=241$) with different location, day, and time. Overall results implied that the application of the proposed algorithm in near-sea-level Langley calibration is proven feasible for AOD measurement.

ABSTRAK

PEMBANGUNAN ALGORITMA PENENTUKURAN LANGLEY BERHAMPIRAN PARAS LAUT BAGI PENGUKURAN KEDALAMAN OPTIK AEROSOL

Kedalaman optik aerosol (AOD) mewakili jumlah penyusutan sinaran cahaya daratan yang disebabkan oleh aerosol. Dalam pemantauan jangka panjang, pengukuran AOD yang tepat adalah sukar kerana penentukuran kerap spektrometer jarang dilakukan. Ini adalah disebabkan kaedah konvensional penentukuran Langley biasanya dilakukan di gunung yang tinggi untuk suasana jelas dan stabil tetapi akses ke kawasan tanah tinggi adalah tidak cekap dari segi kemudahan dan ekonomi. Oleh itu, objektif utama tesis ini adalah untuk membina algoritma penentukuran Langley di tapak berhampiran paras laut bagi pengukuran AOD supaya penentukuran kerap boleh dilaksanakan walaupun di kawasan rendah. Algoritma ini menggunakan gabungan model Perez-Du Mortier (PDM) dan penapis statistik untuk mengekang ekstrapolasi Langley bagi mendapatkan pemalar ruang angkasa yang setepat mungkin dalam pelbagai panjang gelombang. Seterusnya, untuk mengawal ralat hasil daripada respon instrumen fasid, kaedah Nisbah Langley telah digabungkan dengan algoritma tersebut untuk meningkatkan ketepatan ramalan. Melalui cara ini, nilai AOD yang lebih jitu boleh dianggarkan dengan menganalisis semula data spektral yang telah ditentukur menggunakan Hukum Beer-Lambert. Dalam kajian ini, sebanyak 568 data solar spektral telah dikumpulkan dengan menggunakan spektrometer berasaskan tanah bagi tujuan pengesahan. Ia didapati bahawa hasil ramalan AODs bersetuju baik dengan nilai-nilai rujukan yang diperolehi daripada model i-SMARTS dengan kolerasi tinggi dan ralat kecil <3% bagi semua panjang gelombang. Algoritma ini juga telah disahkan konsisten dengan keputusan yang baik pada dua kawasan kajian (n=241) yang berlainan dari segi lokasi, hari, dan masa. Keseluruhannya, keputusan kajian ini menyimpulkan bahawa penggunaan algoritma dalam penentukuran Langley pada kawasan berhampiran laut terbukti sesuai bagi pengukuran AOD.

TABLE OF CONTENTS

	Page
TITLE	i
DECLARATION	ii
CERTIFICATION	iii
ACKNOWLEDGEMENT	iv
ABSTRACT	v
ABSTRAK	vi
TABLE OF CONTENTS	vii
LIST OF TABLES	x
LIST OF FIGURES	xii
LIST OF SYMBOLS	xv
CHAPTER 1: INTRODUCTION	1
1.1 Aerosol Basic: Definition, Sources, and Size Distributions.	1
1.2 Impacts of Atmospheric Aerosol on Climate and Human Health	4
1.2.1 Direct and Indirect Aerosol Effects on Climate	4
1.2.2 Aerosol Human Health Effects	5
1.3 Measurement of Aerosol Optical Depth	6
1.4 Problem Statement	7
1.5 Research Objective	9
1.6 Thesis Contribution	9
1.7 Thesis Arrangement	10
CHAPTER 2: LITERATURE REVIEW	12
2.1 Introduction	12
2.2 Fundamental Theory of Aerosol Absorption and Scattering	12
2.2.1 Optical Properties of an Ensemble Spherical Particle	15
2.3 Review of Aerosol Optical Depth Retrieval Method	17
2.3.1 Retrieval with Satellite Data	17
2.3.2 Retrieval with Ground-Based Radiometer	22

2.3.3	Retrieval with Airborne Radiometer	26
2.3.4	Retrieval with Lidar	27
2.4	The Governing Factors of Aerosol Optical Depth Measurement	30
2.4.1	Sources of Uncertainty	34
2.4.2	Economical Aspect	38
2.5	Conventional Langley Calibration Method	40
2.6	Historical Development of Langley Calibration Method	44
2.6.1	Basic Sunphotometry Langley Method	45
2.6.2	Circumsolar Langley Method	46
2.6.3	Cloud-Screened Langley Method	48
2.6.4	Maximum Value Composite (MVC) Langley Method	52
2.6.5	Comparative Langley Method	53
 CHAPTER 3: RESEARCH METHODOLOGY		 56
3.1	Introduction	56
3.2	Preliminary Instrument Testing	56
3.2.1	Wavelength Verification	59
3.2.2	Spectral Intensity Verification	60
3.3	Development of Near-Sea-Level Langley Calibration Algorithm	61
3.3.1	Clear-Sky Detection Model	61
3.3.2	Statistical Filter	64
3.4	Near-Sea-Level Langley Calibration Experiment	64
3.4.1	Solar Spectral Measurement	65
3.4.2	Implementation of the Proposed Calibration Algorithm	69
3.4.3	Retrieval of Spectral AOD	71
3.5	Performance Analysis of the Proposed Algorithm	72
3.5.1	Validation Analysis using i-SMARTS AOD Inversion Technique	72
3.5.2	Consistency Analysis of the Algorithm	74
 CHAPTER 4: RESULTS & DISCUSSION		 77
4.1	Introduction	77
4.2	Instrument Testing Results	77

4.2.1	Background Noise Correction	77
4.2.2	Wavelength Verification Results	78
4.2.3	Spectral Intensity Verification Results	80
4.3	Langley Calibration at Near-Sea-Level	81
4.3.1	Determination of Extraterrestrial Constant from Langley Plot	81
4.3.2	Data Analysis of the Predicted Spectral AOD	86
4.4	Improved PDM Algorithm using Ratio Langley Method	92
4.4.1	Statistical Comparison between Corrected and Reference AOD	93
4.4.2	Overall Uncertainty Analysis of the Proposed Calibration Algorithm	99
4.5	Consistency Analysis of the Improved PDM Calibration Algorithm	101
 CHAPTER 5: CONCLUSION		107
5.1	Overview	107
5.2	Recommendation	108
 REFERENCES		110
LIST OF PUBLICATIONS		121



LIST OF TABLES

		Page
Table 2.1	Overall comparisons between AOD retrieval methods.	32
Table 2.2	Sources of uncertainty for each retrieval method.	35
Table 2.3	Estimated cost for each retrieval method based on different instruments.	38
Table 3.1	Specification of ASEQ spectrometer.	57
Table 3.2	Calculation of appropriate resistance loading for each LED.	57
Table 3.3	Spectral information of each LED provided by the manufacturer ROHM in datasheet.	60
Table 3.4	Perez model classification of sky condition (Djamila et al., 2011).	62
Table 3.5	Du Mortier model classification of sky condition (Zain-Ahmed et al., 2002).	63
Table 4.1	Comparison of peak wavelength between measured and reference value.	79
Table 4.2	Resulting Langley plots after PDM and statistical filtration, n represents remaining data points where total initial point is 730, R2 is correlation coefficient.	85
Table 4.3	Determination of calibration factor, k using ASTM G173-03 Reference Spectra.	85
Table 4.4	Truncated data of predicted optical depths using the proposed calibration algorithm over study area TMT, KK in Apr – May 2012 (Total data n=568).	87
Table 4.5	Truncated data of reference optical depths simulated using i-SMARTS model over study area TMT, KK in Apr-May 2012 (Total data=568).	88
Table 4.6	Statistical comparison between predicted and reference AODs over study area TMT, KK.	90
Table 4.7	Statistical comparison between corrected and reference AODs over study area TMT, KK.	94

Table 4.8	Truncated data of error estimation between corrected and reference AODs over study area TMT, KK in Apr-May 2012 (Total data n=568).	96
Table 4.9	Overall justification of the proposed calibration algorithms.	100
Table 4.10	Results comparison with other normally calibrated spectrometers.	100
Table 4.11	Truncated data of corrected and reference AOD over study area SST, UMS Kota Kinabalu in Jul-Aug 2012 (Total data n=241).	102
Table 4.12	Statistical comparison between corrected and reference AODs over study area SST, UMS.	105



UMS
UNIVERSITI MALAYSIA SABAH

LIST OF FIGURES

		Page
Figure 1.1	Idealized number and volume distribution of atmospheric aerosols	2
Figure 1.2	Idealized schematic of the sources and sink of primary and secondary aerosols	3
Figure 2.1	Simplified visualization of scattering of an incident EM wave by particle	13
Figure 2.2	Intrinsic visualisation of transmission of an extraterrestrial radiation $I_{\lambda,0}$ through an optical path length s_1 and s_2	17
Figure 2.3	This map is based on data from the Moderate Resolution Imaging Spectroradiometer (MODIS), shows average aerosol amounts around the world for 2007 2011.	20
Figure 2.4	Diminution of solar transmission at multiple AOD values from 0 to 1. Simulation is based on urban aerosol model over tropical atmosphere using SMARTS model.	23
Figure 2.5	AERONET networks worldwide and CIMEL sunphotometer – adapted from AERONET NASA in http://aeronet.gsfc.nasa.gov/ .	24
Figure 2.6	Idealized Langley plot at 500nm for multiple AOD values. Simulation is based on urban aerosol model over tropical atmosphere using SMARTS model.	42
Figure 2.7	Comparison between the Langley-plot method (left panel) and the Circumsolar Langley method (right panel) at $\lambda=500\text{nm}$	48
Figure 2.8	Objective cloud-screening algorithm imposed in Langley calibration $\lambda=500\text{nm}$	50
Figure 2.9	Langley plot for the MFRSR 500nm channel. Solid circles represent time periods identified as clear by Long and Ackerman clear-sky detection algorithm	51
Figure 2.10	Comparison between maximum value composite (MVC)	53

	Langley method and conventional Langley method at 500nm channel	
Figure 3.1	Schematic diagram of the LED connection circuit.	58
Figure 3.2	Central wavelength of the emission lines of LEDs obtained in datasheet from SLR-322 series LED lamps manufacturer ROHM.	60
Figure 3.3	Flowchart of the near-sea-level calibration scheme.	65
Figure 3.4	Experimental set-up over the study area Tun Mustapha Tower (116°E, 6°N, 7.844m above sea level).	66
Figure 3.5	Shading disc of 0.09m diameter is held 1m parallel from the sensor to ensure the shading angle Θ_s to the sensor is the same as the viewing angle Θ_v of the sensor.	68
Figure 3.6	Flowchart of the implementation of PDM filtration in repetitive regression algorithm (RRA).	70
Figure 3.7	Synthetic data of DNI from i-SMARTS.	74
Figure 3.8	Experimental set-up over the study area School of Science & Technology, UMS (116°E, 6°N, 20.398m above sea level).	75
Figure 4.1	Uncorrected, background noise and corrected spectra of red LED spectrum measured by ASEQ spectrometer.	78
Figure 4.2	Comparison of measured and reference spectrum for all LEDs in normalized intensity against wavelength.	79
Figure 4.3	Evolution spectra pattern at different values of current in mA for all LEDs (a) red, (b) orange, (c) yellow, (d) green.	80
Figure 4.4	Correlation analysis for normalized luminous intensity at different current in mA for all LEDs (a) red, (b) orange, (c) yellow, and (d) green.	81
Figure 4.5	Langley plot at 470nm (a) before filtration, after filtration using (b) Perez-Du Mortier model ($NI \geq 0.92$ and $\epsilon \geq 1.55$), and (c) statistical filtration.	84
Figure 4.6	Langley plot at (a) 500nm, (b) 550nm, and (c) 660nm after Perez-Du Mortier model and statistical filtration.	84
Figure 4.7	Histogram plot between predicted and reference AOD values	89

	at (a) 470nm, (b) 500nm, (c) 550nm, and (d) 660nm over study area TMT, KK.	
Figure 4.8	Scatter plot between predicted and reference AOD at multiple wavelength (a) 470nm, (b)500nm, (c) 550nm, and (d) 660nm over study area TMT, KK.	90
Figure 4.9	Variation of extraterrestrial constant plotted against number of observation at multiple wavelengths.	91
Figure 4.10	Frequency distribution of corrected and reference AOD for multiple wavelength (a) 470nm, (b) 500nm, (c) 550nm, and (d) 660nm over study area TMT, KK.	94
Figure 4.11	Correlation analysis between corrected and reference AOD at multiple wavelength (a) 470nm, (b) 500nm, (c) 550nm, and (d) 660nm over study area TMT, KK.	95
Figure 4.12	Histogram of FB values between corrected and reference AODs for multiple wavelengths (a) 470nm, (b) 500nm, (c) 550nm, and (d) 660nm over study area TMT, KK.	97
Figure 4.13	Fluctuation of relative error in corrected AODs over study area TMT, KK. The dotted line represents baseline of acceptable error (± 0.03).	98
Figure 4.14	Frequency distribution of corrected and reference AOD for multiple wavelength (a) 470nm, (b) 500nm, (c) 550nm, and (d) 660nm over study area SST, UMS.	103
Figure 4.15	Correlation analysis between corrected and reference AOD at multiple wavelength (a) 470nm, (b) 500nm, (c) 550nm, and (d) 660nm over study area SST, UMS.	104
Figure 4.16	Histogram of FB values between corrected and reference AODs for multiple wavelengths (a) 470nm, (b) 500nm, (c) 550nm, and (d) 660nm over study area SST, UMS.	104

LIST OF SYMBOLS

d	Diameter of aerosol particle
E^i_i	Parallel components of incident electrical field
E^i_r	Perpendicular components of incident electrical field
E^s_i	Parallel components of scattered electrical field
E^s_r	Perpendicular components of scattered electrical field
$S(\theta)$	Amplitude scattering function
$n_n/T_n(\cos\theta)$	Mie angular function
P^i_n	Legendre polynomials
a_n/b_n	Scattering coefficient in the function of size parameter x
I, Q, V, U	Stoke parameters
σ_s	Scattering cross-section of the particle
r	Radius of the particle
Q_e	Efficiencies of extinction due to particle
Q_s	Efficiencies of scattering due to particle
Q_a	Efficiencies of absorption due to particle
x	Size parameter of particle
$N(r)$	Size distribution of particle
K_e	Volume extinction coefficients due to particle
K_s	Volume scattering coefficients due to particle
K_a	Volume absorption coefficients due to particle
$I_{o,\lambda}$	Extraterrestrial irradiance at top-of-atmosphere at wavelength λ
s	Optical path length
$P(r)$	Received power lidar signal at range r
$P_o(r)$	Transmitted power lidar signal at time t_o and range r
c	Velocity of light
η	Pulse duration of lidar signal
A	Effective system received area of lidar signal
r	Range of lidar signal
$B(r)$	Volume backscatter coefficient of the atmosphere
$\sigma(r)$	Attenuation coefficient of the atmosphere

φ	Backscatter-extinction coefficient ratio
S	Distance-corrected backscattered lidar power
τ	Extinction coefficient
h	Height
a	Angstrom's exponent of particle size
β	Angstrom's coefficient of the number of particles
λ	Wavelength
I_{λ}	Direct normal irradiance at ground at wavelength λ
R	Earth-to-Sun distance in astronomical unit (au)
$\tau_{T,\lambda,i}$	Total optical depth of the i -th scatterer at wavelength λ
m_i	Optical air mass of the i -th scatterer
$\tau_{R,\lambda,i}$	Rayleigh optical depth of the i -th scatterer at wavelength λ
$\tau_{O,\lambda,i}$	Ozone optical depth of the i -th scatterer at wavelength λ
$\tau_{a,\lambda,i}$	Aerosol optical depth of the i -th scatterer at wavelength λ
$\tau_{g,\lambda,i}$	Trace gases optical depth of the i -th scatterer at wavelength λ
p	Site's atmospheric pressure
p_o	Mean atmospheric pressure at sea-level
H	Altitude from sea-level
C_o	Ozone concentration in Dobson unit (DU)
P	Uncalibrated pixel
P_o	Extrapolated of uncalibrated pixels at zero air mass
$P_{\alpha(avg)}$	Average of extrapolated of uncalibrated pixels at zero air mass
n	Number of observation
k	Calibration factor
T	Transmission of light passing through medium
l	Thickness of medium
z	Angle of the beam of primary illumination
φ	Optical index or turbidity optical index
F_a^1	Single scattering approximation of the circumsolar intensity in the almucantar of the Sun
μ_o	Cosine of solar zenith angle
\emptyset	Azimuthal angle measured from solar principal plane

ω_o	Single scattering albedo
$P(\cos\theta)$	Normalized phase function at the scattering angle θ
$\Delta\Omega$	Solid viewing angle of the radiometer
F	Measured intensity radiation of the Sun
F_a	Measured intensity radiation in the alumcantar of the Sun
F_o	Extrapolated of measured intensity radiation at zero air mass
SSR	Single scattering ratio
\bar{U}_m	Air molecules of optical depth
\bar{m}	Complex index fraction of aerosol
ω	Ground albedo
θ	Scattering angle
$f(r')$	Relative size distribution of particle radius r'
r'	Particle radius
$M(t)$	Multiplier necessary to produce correct size distribution at some time t
ψ	Constant between two wavelengths of aerosol optical depth
γ	Curvature of Angstrom's exponent
β_μ	Aerosol optical depth at wavelength one micron
V	Voltage supply
V_F	Forward voltage
I_F	Forward current
R	Resistance
R_v	Variable resistance
R_f	Fixed resistance
λ_p	Peak wavelength of the spectrum
σ_λ	Bandwidth of the spectrum
A_{jk}	Area of the curve at j -th to k -th wavelength
$C(\lambda)_{jk}$	Curve spectrum at j -th to k -th wavelength
I_{ed}	Diffuse horizontal irradiance
I_{eg}	Global horizontal irradiance
ϵ	Perez's clearness index
NI	Du Mortier's nebulosity index

I_{dir}	Direct horizontal irradiance
θ_H	Solar zenith angle
$I_{d,cl}$	Diffuse illumination
CR	Cloud ratio
Ar	Rayleigh scattering coefficient in Perez Model
a_a	Solar altitude
σ	Residual standard deviation
$k_{Ray(\lambda)}$	Rayleigh scattering coefficient at wavelength λ
$k_{oz(\lambda)}$	Ozone absorption cross-section at wavelength λ
g	Asymmetry factor
SSA	Single scattering albedo
FB	Fractional bias
P_{pre}	Predicted value
P_{ref}	Reference value
RE	Relative error
MAE	Mean absolute error
$MAFB$	Mean absolute fractional bias
$RMSE$	Root mean square error
$NRMSE$	Normalized root mean square error
R^2	Coefficient of correlation

CHAPTER 1

INTRODUCTION

1.1 Aerosol Basic: Definition, Sources, and Size Distributions.

Aerosols are small solid particles or liquid droplets suspended in air or other gases environment. They can be naturally produced or manmade generated. Natural aerosols are emitted into the atmosphere by natural processes such as sea spray, volcanoes eruptions, windblown dust from arid and semi-arid regions, terrestrial biomass burning and others. Meanwhile, manmade aerosol are generated from combustion or emission from industrial, welding, and vehicle exhaust or produced intentionally for commercial uses (i.e. flame reactor aerosol that produces nanoparticles). They have very limited life time of about a few days to one week. Despite their relatively short life times, they regularly travel over long distances via air trajectories. The transport pathways may vary seasonally and interannually depending on the air-mass altitude (Paul *et al.*, 2011).

Since aerosols have irregular shapes (i.e. aggregated, spherical, fibrous, and others), categorizing them is often based on the diameter of an idealized sphere, or better known as particle size. These sizes range from few nanometers to several tens of micrometers. More specifically, the aerosol particles with diameters $d \leq 0.1 \mu\text{m}$ belong to the nuclei mode, particles with diameter $0.1 \leq d \leq 2.5 \mu\text{m}$ belong to the accumulation mode where all of these aerosol also known as fine particles, and particles with $d \geq 2.5 \mu\text{m}$ are in the coarse mode. Particles in an aerosol are of the same size is known as monodisperse aerosol and this type of aerosol are normally produced in laboratory for specific purposes. Most aerosols particularly atmospheric aerosols are polydisperse, which have a range of particle sizes. Categorization of these aerosols is based on the use of the particle-size distribution.

Figure 1.1 shows the idealized number and volume density distribution of some atmospheric aerosols. The intermediate between nucleation and accumulation is Aitken mode, which makes up the majority of the aerosol mass. Particles in this size range dominate aerosol direct interaction with sunlight of either scattering or absorbing. Particles at the small end of this size range play significant role in interactions with cloud, whereas particles at the large end contribute significantly near dust and volcanic sources, though of much less numerous. The particles of coarse mode are typically of very minor in number mass but high in volume distribution due to large particle size.

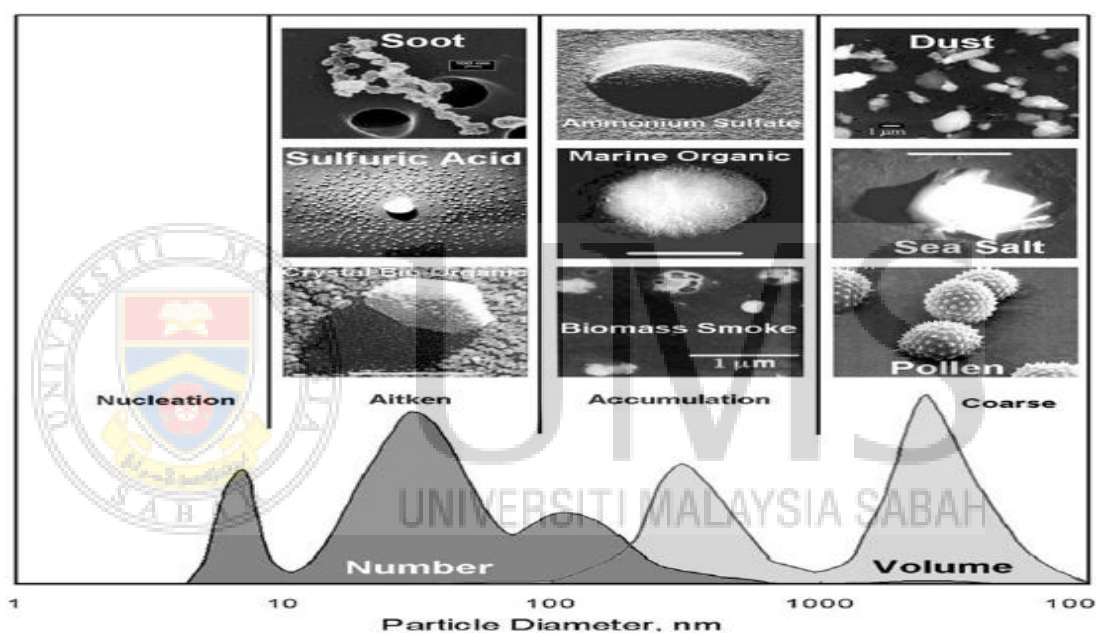


Figure 1.1: Idealized number and volume distribution of atmospheric aerosols

Source : Huang (2009)

Aerosols may further be divided into two broad categories based on their nature of formation: primary and secondary aerosols. Primary aerosols are directly emitted as particles or liquid into the atmosphere by processes occurring on land or water which could be natural or manmade origin. Sources of primary aerosols are sea spray, windblown desert dust, volcanoes, plant particles, biomass burning,

incomplete combustion of fossil fuels and etc. Secondary aerosols, on the other hand, are produced indirectly via atmospheric physical or chemical conversion of gases to particles compounds by nucleation and condensation gases precursors. They are mainly composed of sulphates, carbonaceous particles, nitrates, ammonium and mineral dust of industrial origin (Ghan and Schwartz, 2007).

Figure 1.2 depicts the atmospheric aerosol particle surface weighted by size distribution together with the different mechanisms of aerosol generation. The nuclei range is composed of both primary and secondary aerosols, but physical mechanisms such as condensation and coagulation quickly transform the particle mass from nuclei mode to accumulation mode. These mechanisms are related to their growth and may change their physical and chemical properties (Pöschl, 2005). Besides, the sources and sink for the fine and coarse modes are also different. The fine particles are generally originated from the secondary aerosols and are deposited by rain-wash. Meanwhile, the coarse particles are mainly composed of primary aerosols and sink through sedimentation.

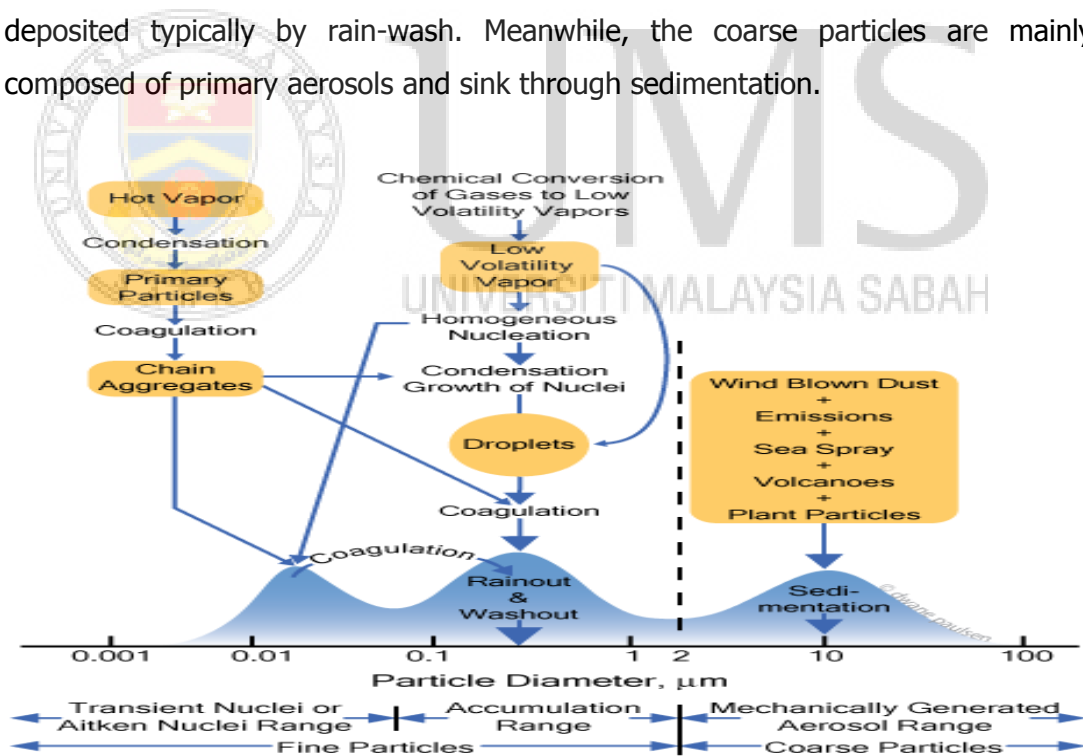


Figure 1.2 : Idealized schematic of the sources and sink of primary and secondary aerosols .

Source : Whitby *et al.* (1972)

1.2 Impacts of Atmospheric Aerosol on Climate and Human Health

Aerosols exert a variety of impacts on environment depending on their properties such as their concentration, size, structure, and chemical composition (Pöschl, 2005). Unlike greenhouse gases, which possesses long life-time and a near-homogeneous spatial distribution, atmospheric aerosols are highly heterogeneous and have limited lifetime of the order of one week in the lower troposphere (Nair *et al.*, 2012). This is because aerosols undergo various physical and chemical interactions and transformations in the atmosphere due to diffusion and aging processes such as nucleation, coagulation, humidification and gas to particle phase conversion (Chaâbane *et al.*, 2005). These processes change their intrinsic characteristics and thus posing varying effects on environment. The two main concerns of aerosol effects are impacts on climate and human health, which are briefly discussed in the following.

1.2.1 Direct and Indirect Aerosol Effects on Climate

In general, aerosol effects on climate can be classified as direct and indirect with respect to radiative forcing of the climate system. Radiative forcing is changes in the energy flux of solar terrestrial radiation in the atmosphere, induced by anthropogenic or natural changes in atmospheric composition, Earth surface properties, or solar activity. Firstly, most of aerosols are highly reflective, they increase the albedo of the earth and thereby cooling the surface and effectively offsetting greenhouse gas warming by about 25% to 50% (Kiehl *et al.*, 2000). This is described as the direct effect which makes the atmosphere brighter when viewed from space since much of Earth's surface is covered by dark oceans and aerosols also scatter visible light backing into space.

Secondly, aerosols in the low atmosphere act as sites at which water vapor can accumulateduring cloud droplet formation, serving as cloud condensation nuclei (CCN). Any change in number concentration or hygroscopic properties of such particle has potential to modify physical and radiative properties of cloud. In this case, the indirect effects of aerosol include an increase in cloud brightness, a reduction in precipitation and an increase in cloud lifetime. These indirect effects were first shown by Twomey (1974) that pollution can lead to an increase in solar

radiation reflected by clouds. The influence of aerosol in this matter lies in the mechanism that the process of cloud condensation causes some of the particles in atmosphere to grow into cloud droplets. These growing particles have typically larger cross-sectional area than the nucleating particles. On the whole, the overall effect is a great magnification of the light scattering power of those particles and resulting in a negative radiative forcing at top of atmosphere (TOA) (Lohmann, 2006).

The scattering and absorption of radiation by aerosols can also cause perturbation in Earth's energy balance in a semi-direct effect (Yu *et al.*, 2006). The effects of this are twofold: warming the atmosphere and cooling the surface below. For instance, black carbon or biomass burning aerosols are absorbing aerosols that absorb incident sunlight and re-radiate at infrared wavelength to cause positive radiative forcing and contributing to global warming (Mishchenko *et al.*, 2007). In contrast, negative radiative forcing type aerosols are sulphate, nitrate and organic carbon particles which causes atmospheric and surface cooling by reflecting solar radiation back to space (Myhre *et al.*, 2009). In this way, an overall effect includes of reducing the atmosphere vertical temperature gradient and therefore contributing to the reduction of formation of convective cloud.

Finally, aerosol are also highly interactive with other components of the climate system, for instance, acidification of lakes and forests through the deposition of sulfates and nitrates and reduction of snow and ice albedo through the deposition of black carbon (Ghan and Schwartz, 2007). Also reported in renewable energy application is the most important variable that conditions the accuracy of the predicted spectra under cloudless skies is aerosol optical depth (AOD) (Gueymard, 2008), which directly constitutes the performance of solar photovoltaic technology.

1.2.2 Aerosol Human Health Effects

Excessive inhalation of particulate matter by human is detrimental to asthma, lung cancer, cardiovascular issues, birth defects, and more severely premature death. Large particles are typically filtered in the nose and throat via cilia or mucus but